nature physics

LETTERS

PUBLISHED ONLINE: 2 FEBRUARY 2015 | DOI: 10.1038/NPHYS3234

Dynamics and inertia of skyrmionic spin structures

Felix Büttner[1,2,3†], C. Moutafis[4★†‡], M. Schneider[3], B. Krüger[1], C. M. Günther[3], J. Geilhufe[5], C. v. Korff Schmising[3], J. Mohanty[3‡], B. Pfau[3], S. Schaffert[3], A. Bisig[1], M. Foerster[1], T. Schulz[1], C. A. F. Vaz[1,6], J. H. Franken[7], H. J. M. Swagten[7], M. Kläui[1] and S. Eisebitt[3,5]

Skyrmions are topologically protected winding vector fields characterized by a spherical topology[1]. Magnetic skyrmions can arise as the result of the interplay of various interactions, including exchange, dipolar and anisotropy energy in the case of magnetic bubbles[2–4] and an additional Dzyaloshinskii–Moriya interaction in the case of chiral skyrmions[5]. Whereas the static and low-frequency dynamics of skyrmions are already well under control[6–9], their gigahertz dynamical behaviour[2] has not been directly observed in real space. Here, we image the gigahertz gyrotropic eigenmode dynamics of a single magnetic bubble and use its trajectory to experimentally confirm its skyrmion topology. The particular trajectory points to the presence of strong inertia, with a mass much larger than predicted by existing theories. This mass is endowed by the topological confinement of the skyrmion and the energy associated with its size change. It is thereby expected to be found in all skyrmionic structures in magnetic systems and beyond. Our experiments demonstrate that the mass term plays a key role in describing skyrmion dynamics.

Skyrmion configurations are pervasive in nature and have been observed in a wide variety of research areas in physics[1–15]. By definition, skyrmions are vector fields that can be continuously wrapped around a sphere and the number of times the sphere is covered during this continuous deformation is the skyrmion number N. It can be shown that skyrmions are always confined in all spatial directions (see Fig. 1 and Supplementary Information I). Magnetic skyrmions are promising candidates for current-driven memory devices[14,15] owing to their high mobility at ultralow current densities[7]. The static manipulation of magnetic skyrmions (nucleation, stability, and annihilation) is now well under control (see refs 8,15 and further references in Supplementary Information VII); however, their intrinsic high-frequency dynamics has thus far not been directly observed in real space, and previous experimental investigations have not allowed the determination of inertial effects[6,16]. Furthermore, a number of existing theoretical descriptions using quasiparticle models of magnetic skyrmions neglect inertia[6,17,18]. Inertial effects are visible only at frequencies comparable to or faster than those intrinsic to the system (for example, the Larmor frequency), which are in the gigahertz regime in the case of solid-state magnetism. Consistently, it is expected from numerical simulations that the gigahertz gyrotropic motion of skyrmionic spin systems exhibits the characteristics of inertia[2,19] through the existence of two gyrotropic eigenmodes, one clockwise and one anticlockwise (massless skyrmions have just one gyrotropic eigenmode, see Supplementary Information II). However, only one of these modes has been observed so far[16]. Here, we observe that the skyrmion motion is indeed composed of two eigenfrequencies, and we also use this effect to experimentally determine the mass of a skyrmionic magnetic quasiparticle. We observe that this mass is sizable and, in fact, much larger than masses found for other magnetic quasiparticles[20–22]. Such a large mass, which significantly exceeds theoretical predictions[19], has a fundamental impact on the dynamical behaviour of magnetic skyrmions, especially in the technologically important case of magnetic thin-film nanostructures, as we show in this work.

The presence of the inertial mass originates from the ability of the system to store energy internally during its motion[2,19]; in our system this is achieved through a deformation in shape, a feature which we expect to be common to all confined (meta-)stable structures. Such deformations are visible in simulations of bubbles[2] as well as of chiral skyrmions[11] (see Supplementary Information II). Inertia of domain walls, confined in one dimension and extended in the other, has been known for a long time[23]. Domain wall inertia causes retardation, but does not change the trajectory of the wall dynamics[24]. In contrast, as shown in this Letter, fully confined skyrmions exhibit an additional topological source of inertia that makes the effective mass very large in comparison to straight domain walls and induces fundamental changes to their trajectory.

The experiment is performed using time-resolved pump–probe X-ray holography[25,26] to image the gyrotropic trajectory of a skyrmionic magnetic bubble (a skyrmion stabilized by dipolar energies, a 'skyrmion bubble') in a sub-micrometre diameter magnetic disk (Fig. 2a) after a magnetic field gradient excitation. A static out-of-plane field of −120 mT is applied, resulting in a ground state with two bubbles. Both bubbles are several radii away from the edge of the disk; thus, interactions with this edge can be neglected. Rather, the bubbles are subjected to a local magnetic potential, which originates from static irregularities of the material structure

[1]Institute of Physics, Johannes Gutenberg-Universität Mainz, Staudinger Weg 7, 55128 Mainz, Germany. [2]Graduate School of Excellence Materials Science in Mainz, Staudinger Weg 9, 55128 Mainz, Germany. [3]Institut für Optik und Atomare Physik, Technische Universität Berlin, Straße des 17. Juni 135, 10623 Berlin, Germany. [4]Swiss Light Source, Paul Scherrer Institut, 5232 Villigen PSI, Switzerland. [5]Helmholtz-Zentrum Berlin für Materialien und Energie GmbH, Hahn-Meitner-Platz 1, 14109 Berlin, Germany. [6]SwissFEL, Paul Scherrer Institut, 5232 Villigen PSI, Switzerland. [7]Department of Applied Physics, Center for NanoMaterials, Eindhoven University of Technology, PO Box 513, 5600 MB Eindhoven, The Netherlands. †These authors contributed equally to this work. ‡Present addresses: Nano Engineering & Storage Technology Group, School of Computer Science, University of Manchester, Manchester M13 9PL, UK (C.M.); Department of Physics, Indian Institute of Technology Hyderabad, Ordnance Factory Estate, Yeddumailaram, Andhra Pradesh 502205, India (J.M.). ★e-mail: christoforos.moutafis@manchester.ac.uk

of the magnetic film and from (possibly dynamic) interactions with the domain pattern in the disk. The excitation of this skyrmionic state is achieved by injecting bipolar current pulses into a microcoil enclosing the disk, generating an out-of-plane field pulse. The time evolution of the current pulse is plotted in Fig. 2b, and the field generated at the pulse peak is visualized in the inset of Fig. 2d. A positive current generates a field which is antiparallel to the negative static bias field, favouring the growth of the bubble domains and the nucleation of new reverse domains.

Selected images acquired at different times after the start of the pulse are presented in Fig. 2c. To generate the required field gradient to displace bubbles, we apply a positive field pulse to nucleate a third domain at an artificial notch-shaped nucleation centre at the top of the disk, and we use the strong (and ultrafast) gradient of the stray field created by this domain to dynamically alter the potential landscape and subsequently displace one of the two bubbles (further referred to as 'the bubble') sufficiently for experimental observation. Field gradients of this magnitude (expected to be of the order of $\mathrm{T\,\mu m^{-1}}$)[2] are otherwise experimentally inaccessible, in particular with rise times of only a few hundred picoseconds. After reversal of the field pulse, the third domain annihilates through the intermediate formation of an $N=0$ bubble. The bubble subsequently returns to its equilibrium position. The other bubble in the disk does not move because it is pinned in a strong potential minimum. The interaction with the first bubble is therefore purely static, and the relaxation of this first bubble is thus fully analogous to the motion of a bubble in the static potential defined by the edge of a disk, which has been studied in previous theoretical work[2,19]. The full video of the bubble motion and comprehensive discussions of further details of the magnetization dynamics in the disk can be found in Supplementary Information III.

The full trajectory of the bubble, plotted in Fig. 2d, forms a loop with clearly distinct excitation and relaxation paths. In particular, after $t=4.5$ ns, the bubble moves on a spiralling trajectory, an unequivocal signature of the influence of the gyrocoupling vector and hence of a non-zero skyrmion number. In materials with preferred out-of-plane spin alignment, all fully confined objects (that is, domains that do not touch the sample boundary) are configurations with integer N; specifically, from micromagnetic simulations we deduce that the observed bubble has unity N because all $|N|\neq 1$ configurations that could be expected for a bubble in this material show very complex trajectories (see ref. 2 and Supplementary Information IV). As we know the direction of the applied magnetic field, we also know the polarity of the bubble and thus its skyrmion number $N=+1$.

Our experiment constitutes the first direct experimental observation of gigahertz dynamics of a skyrmionic spin structure, which was made feasible as a result of our extremely high accuracy in tracking the centre of the bubble (of better than 3 nm). This outstanding accuracy for time-resolved experiments can be reached with X-ray holography because the imaging process is intrinsically insensitive to drift[25,26]. Isolated skyrmions can be imaged even if they are much smaller than the pixel resolution, which is 40 nm in our case. With prospective pixel resolutions of sub-10 nm, imaging of all varieties of skyrmions is expected to be possible with X-ray holography[27].

The observed gyrotropic trajectory is in excellent agreement with the recently proposed theoretical model assigning to the $N=\pm 1$ bubble an inertial mass. The theory predicts a second-order differential equation of motion for the centre of mass $\mathbf{R}$ of the magnetization[19]

$$-M\ddot{\mathbf{R}}+\mathbf{G}\times\dot{\mathbf{R}}+D\dot{\mathbf{R}}-\partial_{\mathbf{R}}U=0 \qquad (1)$$

Here, M is the effective inertial mass, $\mathbf{G}=(0,0,G)$ is the gyrocoupling vector, with $G=-4\pi N t_{\mathrm{Co}} M_{\mathrm{s}}/\gamma$ (where t_{Co} is the total magnetic material thickness, M_{s} its saturation magnetization and $\gamma=1.76\times 10^{11}\,\mathrm{A\,s\,kg^{-1}}$ the gyromagnetic ratio), D is the dissipation tensor and U is the magnetostatic potential, which we approximate to be parabolic $\partial_{\mathbf{R}}U=K\mathbf{R}$. The general solution of this equation is a superposition of two damped spiralling motions, one clockwise (CW) and one anticlockwise (ACW). The parameters of this general solution are extracted from a fit to the experimental data (see Supplementary Information IX for the fitting details).

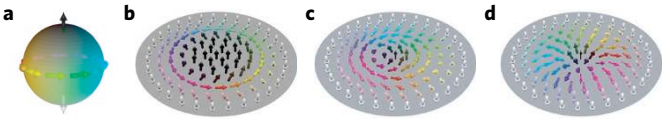

Figure 1 | Illustration of the topology of skyrmionic spin structures with a disk-shaped domain space. a, A sphere S^2 with its identity map vector field into which all skyrmions can be continuously deformed. It is also the most general representation of the spin space (because spin is a vector in $\mathbb{R}^3$ with constant modulus). The hue of the colour represents the azimuthal angle φ, and the black and white colour represents the polar angle θ of the spherical coordinates. **b**, A magnetic bubble, which covers the sphere exactly once ($N=1$). The poles are mapped to extended areas (the inner and outer domains). Hence, all spins at the boundary of the domain space point in the same direction, which confines the inner domain and the domain wall. This is the structure investigated in the present work. **c**, A chiral skyrmion, which has a different radial distribution from that of the bubble[5]. Topologically, however, both are the same, as the bubble can be obtained from the chiral skyrmion by expanding its inner domain. **d**, A hedgehog skyrmion, which is again topologically equivalent to the other figures. The hedgehog skyrmion can be continuously deformed to the chiral skyrmion by rotating all spins by 90° around an axis normal to the plane.

The theoretical model given by equation (1) accurately describes the gyrotropic part of the observed trajectory $\mathbf{R}(t)=(X(t),Y(t))$. This is visualized in Fig. 3, showing the projections $X(t)$, $Y(t)$ and $Y(X)$ in a, b and c, respectively. A good fit to the data, visualized by a solid, coloured line in Fig. 3, is possible only with a globally simultaneous, coherent superposition of two gyrotropic modes: a CW higher-frequency mode and a ACW lower-frequency mode. This confirms the presence of an inertial mass, because, without the mass term, the sense of gyration would be fixed by G (which is a constant of motion) and only one mode could be excited at a time. For comparison, the best fit of the trajectory of a massless bubble is illustrated in Fig. 3 by a grey line, showing that the mass term is necessary to describe the data. The excellent agreement with the theoretical model furthermore confirms the validity of the parabolic approximation for the potential used, see Supplementary Information V.

From the fit we obtain the frequencies $\omega_1=1.00(13)$ GHz (ACW mode) and $\omega_2=-1.35(16)$ GHz (CW mode, as indicated by the minus sign). The frequencies of both modes are in the gigahertz regime, which is in line with numerical predictions in ref. 2. The same characteristic spectrum of one CW and one ACW mode, with very similar frequencies, has been predicted by numerical simulations for chiral skyrmion crystals, underlining the fundamental topological origin of the gyrotropic motion and of the presence of inertia[11]. The inertial mass of the bubble is inversely proportional to the sum of the two frequencies[19], which allows us to derive a lower limit $|M_{\mathrm{LL}}|>8\times 10^{-22}$ kg for the inertial mass with high confidence (5σ) despite the relatively large experimental uncertainties for the frequencies. From the product of the frequencies we obtain the stiffness $K=3.5(16)\times 10^{-3}\,\mathrm{N\,m^{-1}}$ of the local magnetostatic potential.

The lower limit for the mass of the bubble corresponds to an areal mass density of $2.0(4)\times 10^{-7}\,\mathrm{kg\,m^{-2}}$. Such large inertia has been reported so far only for cross-tie domain walls[28]. It is at least two orders of magnitude larger than any value previously

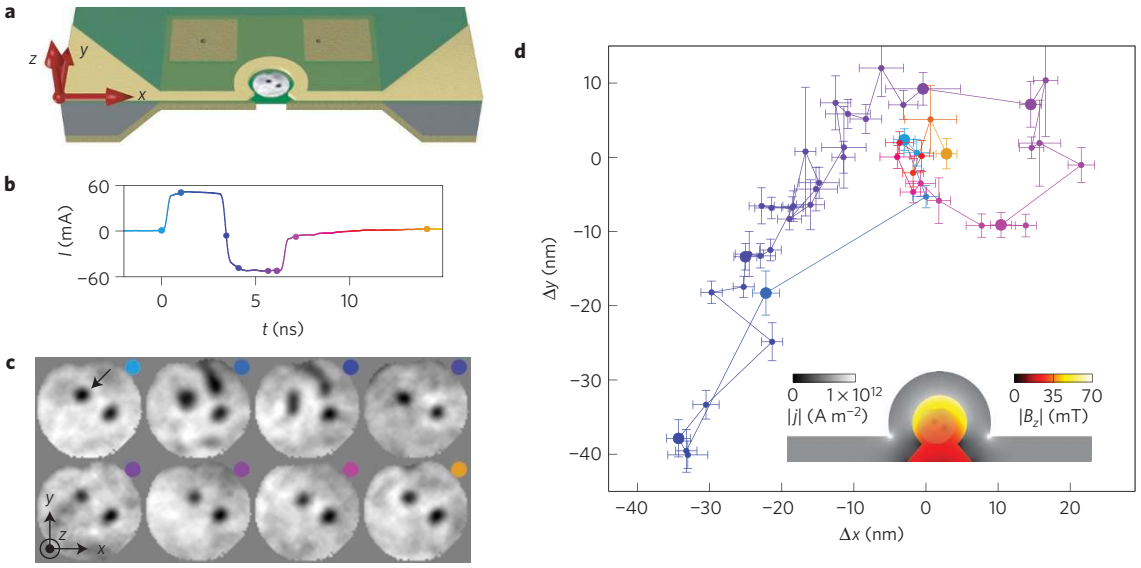

Figure 2 | Excitation of a multi-bubble state by an external magnetic field pulse. a, Schematic cross-section of the sample, showing the pump and the imaging elements on the Si_3N_4 membrane (light green), which is supported by a Si frame (grey). The 550 nm diameter magnetic disk (in the centre) is surrounded by a Au microcoil (bright yellow). The back side of the membrane is covered by a Au mask (dark yellow) with three holes, one with 800 nm diameter behind the magnetic CoB/Pt disk and two reference holes at a few μm distance. **b**, Temporal evolution of the injected current generating the magnetic field pulse. The colour of this plot represents the time delay, and is used consistently throughout this paper. **c**, Magnetic domain configuration of the disk at different time delays, as indicated by the coloured point in each image. In the black areas the magnetization is antiparallel to the static field (that is, the magnetization is pointing towards the reader), whereas in the white areas it is parallel. **d**, Displacement (Δx, Δy) of the centre of magnetization of the bubble indicated by an arrow in **c**, with the time encoded by the colour of the points. Large diameter dots correspond to the images shown in **c**. The line connecting the points is a guide to the eye, visualizing the temporal sequence of the measured data. It does not represent the motion of the bubble. The error bars represent one standard deviation, obtained from the difference of the bubble positions in the two independent reconstructions plus a constant noise level of 1.4 nm (see Supplementary Information IX for details). The inset shows a finite difference calculation of the current density in the microcoil and the corresponding z-component of the generated magnetic field inside the coil for a current of 52 mA.

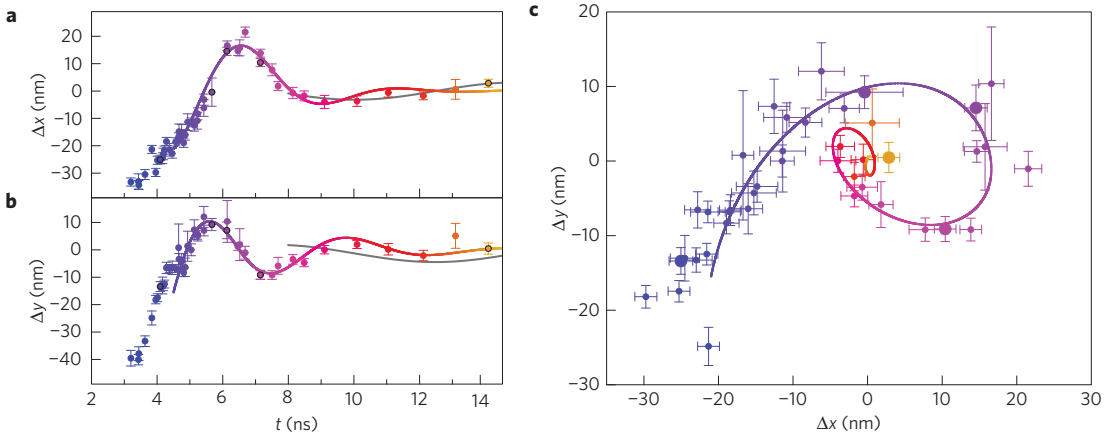

Figure 3 | Analytic description of the gyrotropic motion of the bubble. a,**b**, Displacements Δx and Δy of the x and y coordinate of the centre of magnetization of the bubble versus time. **c**, Trajectory of the bubble. Coloured lines in **a**–**c** represent a fit of the analytical model to the experimentally observed bubble gyration (points). The colour encodes the time after the start of the bipolar pulse (see Fig. 2b). Large-diameter dots correspond to the images shown in Fig. 2c. The grey lines in **a**,**b** show the best fit with a single-frequency model to the data after $t = 8$ ns, which is not able to describe the data. Error bars represent standard deviation, see Fig. 2d.

reported for straight domain walls[20–22], and a factor of five larger than predicted by the theory in ref. 19 (for details, see Supplementary Information VI). Such a large mass is responsible for the enormous deviation of our measured trajectory from the best fit with a massless model (Fig. 3). The impact of the mass is also significant in other geometries, such as the recently suggested case of a skyrmion in a wire[14,15]. Here, the mass helps to avoid the transversal expulsion of the skyrmion from the wire, thus leading to higher longitudinal displacements per pulse, as demonstrated in Supplementary Information VII.

The amplification of inertia in confined, low-dimensional spin structures by up to two orders of magnitude is known from Bloch lines and has been attributed to the local exchange energy[6]. Here, we attribute the surprisingly large mass of magnetic skyrmions to an additional energy reservoir associated with a change of its size (breathing mode, see Supplementary Information II)—that is, to a collective or emergent source of inertia. Such a breathing mode is inherent to all structures that are of finite extent in thermodynamic equilibrium (in magnetism always objects with integer N topology), where energy can be stored by a change in

the spatial extent. The breathing mode mass is associated with the $N = 1$ topology, because $N = 1$ structures are the only ones that exhibit the gyrotropic eigenmodes described by equation (1). We therefore call the mass, arising from the specific topology, a topological mass. The particularly large mass found in magnetic skyrmions is related to the strong dipolar energy of the breathing mode. The non-local breathing mode energy is not included in the Döring mass and has thus been neglected in previous theoretical models[19], but contributes significantly to the mass found here. The previously found large mass of cross-tie walls can actually be attributed to their local skyrmionic spin structure[13,29]. A broad range of simulations indicates that the mass density of a skyrmion is not modified by any environmental factor changing its spatial extent (see Supplementary Information V). Therefore, the large skyrmion mass found by us is expected to dominate the skyrmion motion independently of the device geometry. We anticipate that this topological mass provides an important possibility to tailor the dynamical behaviour of skyrmions and to facilitate their application in future devices.

Methods

The sample was prepared as described in refs 26,30, with a $Pt(2)/[Co_{68}B_{32}(0.4)/Pt(0.7)]_{30}/Pt(1.3)$ (thickness in nm) magnetic layer patterned onto a 550 nm disk with a notch at the top, a Au microcoil tightly around the disk (see Fig. 2a), and two reference holes with diameters of 80 nm and 55 nm. The magnetic imaging was performed using time-resolved X-ray holography at the UE52-SGM beamline at BESSY II in Berlin, Germany. Bipolar rectangular microwave pulses with a current of 52 mA were injected into the microcoil at a repetition rate of 1.25 MHz, synchronized to the probe X-rays (Fig. 2b). The resulting field, estimated using finite difference calculations, was roughly homogeneous in the out-of-plane direction (inset Fig. 2d), with a strength of $B_z = -35$ mT at the position of the bubble at maximum negative current, and small in-plane components $B_x = -1.5$ mT and $B_y = 6.5$ mT. The residual field gradient was $\partial_x B_z = 8.7\,\mu T\,nm^{-1}$ and $\partial_y B_z = -45\,\mu T\,nm^{-1}$, pushing the bubble towards the centre of the disk. The magnetic domain configuration was imaged at variable time delays t with a temporal resolution of 50 ps (standard deviation), determined by the duration of the synchrotron X-ray pulses and their temporal jitter with respect to our electronics. For each time delay, the pump–probe experiment was repeated about 10^9 times, corresponding to a total number of $6.4(5) \times 10^7$ recorded photons of each helicity (positive and negative) per image. Images were recorded in a random non-chronological order.

In the reconstructed real-space magnetic image, the area of the disk was cropped using the topographic information in the holograms. The centre of the bubble was calculated by statistical means. By recording Fourier space information, the real-space reconstruction is inherently drift free. Therefore, we can determine the position of the centre of the bubble with an average precision of 2.3 nm, which is much better than the approximate spatial resolution of 40 nm (ref. 30).

Received 24 July 2014; accepted 17 December 2014; published online 2 February 2015

References

1. Skyrme, T. A unified field theory of mesons and baryons. *Nucl. Phys.* **31,** 556–569 (1962).
2. Moutafis, C., Komineas, S. & Bland, J. A. C. Dynamics and switching processes for magnetic bubbles in nanoelements. *Phys. Rev. B* **79,** 224429 (2009).
3. Moutafis, C. *et al.* Magnetic bubbles in FePt nanodots with perpendicular anisotropy. *Phys. Rev. B* **76,** 104426 (2007).
4. Yu, X. *et al.* Magnetic stripes and skyrmions with helicity reversals. *Proc. Natl Acad. Sci. USA* **109,** 8856–8860 (2012).
5. Rößler, U. K., Bogdanov, A. N. & Pfleiderer, C. Spontaneous skyrmion ground states in magnetic metals. *Nature* **442,** 797–801 (2006).
6. Malozemoff, A. P. & Slonczewski, J. C. *Magnetic Domain Walls in Bubble Materials* (Academic Press, 1979).
7. Schulz, T. *et al.* Emergent electrodynamics of skyrmions in a chiral magnet. *Nature Phys.* **8,** 301–304 (2012).
8. Romming, N. *et al.* Writing and deleting single magnetic skyrmions. *Science* **341,** 636–639 (2013).
9. Nagaosa, N. & Tokura, Y. Topological properties and dynamics of magnetic skyrmions. *Nature Nanotech.* **8,** 899–911 (2013).
10. Battye, R. A., Cooper, N. R. & Sutcliffe, P. M. Stable skyrmions in two-component Bose–Einstein condensates. *Phys. Rev. Lett.* **88,** 080401 (2002).
11. Mochizuki, M. Spin-wave modes and their intense excitation effects in skyrmion crystals. *Phys. Rev. Lett.* **108,** 017601 (2012).
12. Yu, X. Z. *et al.* Real-space observation of a two-dimensional skyrmion crystal. *Nature* **465,** 901–904 (2010).
13. Komineas, S. Rotating vortex dipoles in ferromagnets. *Phys. Rev. Lett.* **99,** 117202 (2007).
14. Fert, A., Cros, V. & Sampaio, J. Skyrmions on the track. *Nature Nanotech.* **8,** 152–156 (2013).
15. Sampaio, J. *et al.* Nucleation, stability and current-induced motion of isolated magnetic skyrmions in nanostructures. *Nature Nanotech.* **8,** 839–844 (2013).
16. Onose, Y. *et al.* Observation of magnetic excitations of skyrmion crystal in a helimagnetic insulator Cu_2OSeO_3. *Phys. Rev. Lett.* **109,** 037603 (2012).
17. Zang, J., Mostovoy, M., Han, J. H. & Nagaosa, N. Dynamics of skyrmion crystals in metallic thin films. *Phys. Rev. Lett.* **107,** 136804 (2011).
18. Lin, S-Z., Reichhardt, C., Batista, C. D. & Saxena, A. Particle model for skyrmions in metallic chiral magnets: Dynamics, pinning, and creep. *Phys. Rev. B* **87,** 214419 (2013).
19. Makhfudz, I., Krüger, B. & Tchernyshyov, O. Inertia and chiral edge modes of a skyrmion magnetic bubble. *Phys. Rev. Lett.* **109,** 217201 (2012).
20. Rhensius, J. *et al.* Imaging of domain wall inertia in permalloy half-ring nanowires by time-resolved photoemission electron microscopy. *Phys. Rev. Lett.* **104,** 067201 (2010).
21. Bedau, D. *et al.* Detection of current-induced resonance of geometrically confined domain walls. *Phys. Rev. Lett.* **99,** 146601 (2007).
22. Vogel, J. *et al.* Direct observation of massless domain wall dynamics in nanostripes with perpendicular magnetic anisotropy. *Phys. Rev. Lett.* **108,** 247202 (2012).
23. Döring, W. Über die Trägheit der Wände zwischen Weißschen Bezirken. *Z. Naturforsch. A* **3,** 373–379 (1948).
24. Thomas, L., Moriya, R., Rettner, C. & Parkin, S. S. Dynamics of magnetic domain walls under their own inertia. *Science* **330,** 1810–1813 (2010).
25. Eisebitt, S. *et al.* Lensless imaging of magnetic nanostructures by X-ray spectro-holography. *Nature* **432,** 885–888 (2004).
26. Büttner, F. *et al.* Magnetic states in low-pinning high-anisotropy material nanostructures suitable for dynamic imaging. *Phys. Rev. B* **87,** 134422 (2013).
27. Geilhufe, J. *et al.* Monolithic focused reference beam X-ray holography. *Nature Commun.* **5,** 3008 (2014).
28. Bostanjoglo, O. & Rosin, Th. Resonance oscillations of magnetic domain walls and Bloch lines observed by stroboscopic electron microscopy. *Phys. Status Solidi A* **57,** 561–568 (1980).
29. Kuepper, K. *et al.* Dynamic vortex–antivortex interaction in a single cross-tie wall. *Phys. Rev. Lett.* **99,** 167202 (2007).
30. Büttner, F. *et al.* Automatable sample fabrication process for pump–probe X-ray holographic imaging. *Opt. Express* **21,** 30563–30572 (2013).

Acknowledgements

We thank V. Guzenko and the Laboratory for Micro- and Nanotechnology at the Paul Scherrer Institut for access to the clean room, use of the Electron Beam Lithography system, and for support. C.M. thanks J. Raabe and S. Komineas for discussions. We thank the Department of Physics of the University of Hamburg for access to the PHYSnet-Computing Center. This work was funded by the German Ministry for Education and Science (BMBF) through the projects MULTIMAG (13N9911) and MPSCATT (05K10KTB), the EU's 7th Framework Programme MAGWIRE (FP7-ICT-2009-5 257707), the European Research Council through the Starting Independent Researcher Grant MASPIC (ERC-2007-StG 208162), the Mainz Center for Complex Materials (COMATT), the Swiss National Science Foundation (SNF) and the Deutsche Forschungsgemeinschaft (DFG).

Author contributions

C.M., M.K. and S.E. conceived the experiment. F.B., M.S., C.M.G., C.A.F.V. and J.H.F. prepared the samples. F.B., C.M., M.S., C.M.G., J.G., C.v.K.S., J.M., B.P., S.S., A.B., M.F. and T.S. performed the dynamic imaging experiment. The data analysis was carried out by F.B. and B.K. along with discussions with C.M., C.A.F.V., M.K. and S.E. The manuscript was written by F.B. with input from C.M., C.A.F.V., M.K., S.E. and all other authors. Supervision was by H.J.M.S., M.K. and S.E.

Additional information

Supplementary information is available in the online version of the paper. Reprints and permissions information is available online at www.nature.com/reprints. Correspondence and requests for materials should be addressed to C.M.

Competing financial interests

The authors declare no competing financial interests.